Characterization of a Closed-Shell Fluorine−Fluorine Bonding Interaction in Aromatic Compounds on the Basis of the Electron Density

Chérif F. Matta, Norberto Castillo, and Russell J. Boyd*

Department of Chemistry, Dalhousie University, Halifax, Nova Scotia, Canada B3H 4J3

Received: October 30, 2004; In Final Form: February 6, 2005

A bond path linking two saturated fluorine atoms is found to be ubiquitous in crowded difluorinated aromatic compounds. The bond path is shown to persist for a range of internuclear distances (2.3−2.8 Å) and a range of relative orientations of the two C−F internuclear axes. The F···F bonding is shown to exhibit all the hallmarks of a closed-shell weak interaction. The presence of such a bond path can impart as much as 14 kcal/mol of local stabilization to the molecule in which it exists, a stabilization that can be offset or even overwhelmed by destabilization of other regions in the molecule. Several other weak closed-shell interactions were also found and characterized including F···C, F···O, and C···C interactions, hydrogen bonding, dihydrogen bonding, and hydrogen−hydrogen bonding. This study represents another example of the usefulness and richness of the bond path concept and of the theory of atoms in molecules in general.

Introduction

Halogen−halogen "short contacts" of the type C−X···X−C (where X = F, Cl, Br, or I) and contacts of the type C−X···O, C−X···N, C−X···H−(C, N, O), or C−F···M (metal) have long been known in X-ray crystallographic structures (see, for example, refs 1−6 and references therein). In the crystallographic literature, a short contact between two atoms A and B usually signifies that the A···B distance is less than the sum of their van der Waals radii.[7] More recently, several authors have reported weak closed-shell bonding interactions between halogens on the basis of the topological properties of the electron density. For example, Tsirelson et al. have described a closed-shell bonding interaction between chlorine atoms belonging to neighboring molecules in solid molecular chlorine crystals, the interaction that enables solid chlorine to exist in the crystalline form.[8] Bach, Lentz, and Luger[9] have described weak intermolecular C−F···O and C−F···F−C bonding interactions in an electron density study of crystalline pentafluorobenzoic acid at 110 K using multipolar refinement. In a recent theoretical study, Grabowski et al.[10] reported evidence for the presence of intramolecular C−F···F−C and C−F···H−C bonding interactions based on the topology of the electron density in fluorinated styrenes. In another recent work, Alkorta and Elguero[11] found a correlation between the calculated electron density at the C−F···F−C bond critical point (defined in the following section) and the through-space fluorine−fluorine spin−spin coupling constant, J_{FF}, in six fluorinated organic compounds. The same group has also studied the geometries, bond properties, and interaction energies of several classes of nonclassical bonding interactions involving halogens at the density functional theory (DFT) and second-order Møller−Plesset perturbation theory (MP2) levels.[12] We have recently reported correlations of the fluorine−fluorine spin−spin coupling constants with the spatial separation and with the electron delocalization between the two fluorine atoms.[13] During the course of our investigation, we found that relatively strong through-space coupling constants occur in those instances where the two fluorine atoms are linked by a bond path, a line of maximal electron density linking bonded nuclei in space. In previous studies, however, the F···F bonding was either examined for a few molecules or was not the main focus of the investigation. The ubiquity of the F···F bonding interaction, thus, calls for a systematic examination, which is the purpose of the present paper. We have also found several other interesting closed-shell bonding interactions in the course of the present investigation which are described herein.

* To whom correspondence should be addressed. E-mail: russell.boyd@dal.ca. Phone: (902) 494-8883. Fax: (902) 494-1310.

Characterization of Chemical Bonding

The properties of matter are determined by the distribution of electronic charge in space, the electron density, $\rho(\mathbf{r})$. The electron density exhibits a rich topology which can be analyzed within the framework of the theory of atoms in molecules (AIM) to recover familiar chemical concepts such as a bonding interaction.[14,15] The topology of $\rho(\mathbf{r})$ is dominated by the nuclear maxima and by lines of maximum electron density linking the nuclear maxima of bonded nuclei. In an equilibrium geometry, a line of maximal density linking two nuclei is known as the bond path.[14−16] The network of bond paths in a molecule defines the molecular graph which corresponds to the bonded structure deduced from experiment for a wide variety of compounds.[17−19]

The existence of a bond path is an "all or nothing" topological phenomenon: A single bond path connects any two bonded atoms regardless of the bond order or the type of bonding (covalent, ionic, hydrogen, van der Waals, etc.). The presence of a bond path is always accompanied by an interatomic surface (IAS) between the two bonded atoms. The IAS satisfies a strict quantum condition, the zero-flux condition, which partitions the system into "proper open quantum subsystems"[20] and which is expressed by[14]

$$\nabla\rho(\mathbf{r})\cdot\mathbf{n}(\mathbf{r}) = 0, \quad \text{for all } \mathbf{r} \text{ on the surface} \qquad (1)$$

where $\nabla\rho(\mathbf{r})$ is the gradient of the electron density and $\mathbf{n}(\mathbf{r})$ is a unit vector normal to the surface. The zero-flux surface is defined by a particular set of $\nabla\rho(\mathbf{r})$ trajectories all of which

10.1021/jp045044z CCC: $30.25
Published on Web 03/31/2005

terminate at a single point, a critical point in the density (where $\nabla\rho(\mathbf{r}) = 0$), known as the bond critical point (BCP). There is one (and only one) BCP between each pair of atoms that are bonded, that is, linked by a bond path and sharing a common zero-flux IAS. In addition to the set of trajectories which terminate at the BCP and which define the interatomic surface, a pair of trajectories originates at the BCP and each member of this pair terminates at one of the bonded nuclei. This latter pair of trajectories defines the bond path—a line through space along which the density is a maximum with respect to any neighboring line—and the atoms so linked are bonded to one another.[15] The bond path may or may not coincide with the internuclear axis. When the bond path does not coincide with the internuclear axis, the bond path is curved and its length is longer than the internuclear separation (commonly known as the bond length). Curved bond paths typically characterize weaker closed-shell interactions such as hydrogen bonds, the F···F and other interactions reported here, or bonding in strained cyclic molecules. Whenever a bond path links two nuclei, an IAS arises separating their two associated basins. As a corollary, one states that only those atoms that share a common zero-flux IAS are linked by a bond path and, therefore, every pair of bonded atoms is separated by such a surface. Thus, the presence (or absence) of a bond path unambiguously establishes the presence (or absence) of bonding. The ability of the bond path to uniquely trace the molecular graph from the topology of the electron density is of paramount importance in cases of ambiguous bonding,[21,22] as is the case for the bonding interactions that are the subject of this paper.

The properties of the electron (and energy) densities at the BCP have been shown to succinctly characterize bonding interactions in an unambiguous manner.[14,15] Thus, the electron density at the BCP, ρ_{BCP}, provides a measure of the strength of the bonding (or of the bond order) between two atoms. Generally, ρ_{BCP} is >0.20 au for shared or polar interactions and <0.10 au for closed-shell interactions, such as ionic and hydrogen bonding and the interactions examined in this paper.

The Laplacian of the electron density at the BCP, $\nabla^2\rho_{BCP}(\mathbf{r}) = \lambda_1 + \lambda_2 + \lambda_3$, is the sum of the three curvatures of the density at that point: two negative curvatures perpendicular to the bond path (λ_1 and λ_2) and a third positive curvature (λ_3) tangent to the bond path. The sign of the Laplacian of the electron density at the BCP, $\nabla^2\rho_{BCP}(\mathbf{r})$, indicates whether the bonding is of the closed-shell or open-shell type. In a shared interaction, density is accumulated between the nuclei and concentrated along the bond path so that ρ_{BCP} is large and $\nabla^2\rho_{BCP} < 0$ (since the two negative curvatures dominate the small magnitude of the positive curvature). An example of a shared interaction is the C—H bonding for which $\rho_{BCP} = 0.29$ au and $\nabla^2\rho_{BCP} = -1.1$ au. For a closed-shell interaction, density is removed from the region of contact of the two atoms and hence ρ_{BCP} is small and $\nabla^2\rho_{BCP} > 0$, an example being the hydrogen bond N—H···O═C for which $\rho_{BCP} = 0.01$ au and $\nabla^2\rho_{BCP} = +0.03$ au. Polar bonding as in C—X (e.g., X = O, N, or F) exhibits significant charge accumulation between the nuclei typical of shared interactions, but in these cases, the Laplacian can be of either sign (for example, in this study, the $C^{+0.5}$—$F^{-0.6}$ bond is characterized by $\rho_{BCP} = 0.26$ au and $\nabla^2\rho_{BCP} = +0.14$ au). Polar bonding is dominated by charge transfer, and the BCP falls in the region bordering the core of the electropositive atom, unlike shared but nonpolar bonding. These observations lead to the development of a powerful model that predicts atomic and group electronegativity based on the location of the BCP along the bond path.[23,24]

The bond ellipticity, ϵ, measures the preferential accumulation of electron density in a given plane containing the bond path at the BCP. It is defined as $\epsilon = (\lambda_1/\lambda_2 - 1)$, where λ_1 is the perpendicular curvature of greatest magnitude. The ellipticity provides a measure of double bond character, with $\epsilon = 0.0$, 0.23, and 0.45 for the C—C bond in ethane, benzene, and ethene, respectively.

Energy densities at the BCP determined by the one-electron density matrix (as opposed to the density, its diagonal element) summarize the mechanics of a bonding interaction. The AIM theory defines a potential energy density experienced by an electron at position vector $\mathbf{r}$, also known as the virial field, $\mathcal{V}(\mathbf{r})$. The virial field is the average effective potential field felt by an electron in a many-particle system. This field is negative everywhere and when integrated over all space yields the total potential energy of a molecule in an equilibrium geometry. For a stationary state, the virial theorem may be expressed locally:[14,20,25]

$$\left(\frac{\hbar^2}{4m}\right)\nabla^2\rho(\mathbf{r}) = 2G(\mathbf{r}) + \mathcal{V}(\mathbf{r}) \tag{2}$$

where

$$G(\mathbf{r}) = \frac{\hbar^2}{2m}N\int d\tau' \,\nabla\Psi^*\cdot\nabla\Psi \tag{3}$$

is the gradient kinetic energy density in which the symbol $\int d\tau'$ implies the integration over the space coordinates of all electrons but one and summation over all spins, and Ψ is an antisymmetric many-electron wave function. Since it is always true that $G(\mathbf{r}) > 0$ and $\mathcal{V}(\mathbf{r}) < 0$, the local statement of the virial theorem ties in the kinetic and potential energy densities to a term proportional to the Laplacian of the electron density. When the theorem is applied locally at the BCP, interactions for which $\nabla^2\rho_{BCP} < 0$ are dominated by a local lowering of the potential energy, while those for which $\nabla^2\rho_{BCP} > 0$ are dominated by a local excess in the kinetic energy as measured by the 2:1 ratio required for the satisfaction of eq 2. Cremer and Kraka[26] suggested the use of the electronic energy density:

$$H(\mathbf{r}) = G(\mathbf{r}) + \mathcal{V}(\mathbf{r}) \tag{4}$$

evaluated at a BCP ($H_{BCP} = G_{BCP} + \mathcal{V}_{BCP}$) to compare the kinetic and potential energies on an equal footing. The electronic energy density yields the total electronic energy when integrated over all space. H_{BCP} assumes negative values for all interactions with significant sharing of electrons, with its magnitude reflecting the "covalent character" of the interaction.[26]

The presence of a bond path is always stabilizing and is mirrored by a "shadow" path, the virial path, which is a line of maximally negative potential energy density in space linking the nuclei of the two bonded atoms.[27] The appearance of a bond path upon a conformational change entails a local lowering of the energy of the system, even when this fact is disguised by a rise in the total energy caused by other energetic changes in the molecule. For example, it has been shown recently that the twisting of biphenyl is driven by the destabilization of the two carbon atoms connecting the two rings in the planar conformation rather than due to a "steric nonbonded repulsion" between the ortho-hydrogen atoms.[28] In the planar conformation, the ortho-hydrogen atoms are linked by a hydrogen—hydrogen bond path and each is stabilized by 7 kcal/mol as a result. In the planar conformation, the destabilization of the two carbon atoms linking the phenyl rings exceeds the stabilization due to the H···H interaction by a net ~2 kcal/mol when compared

to the twisted equilibrium geometry.[28] Similar hydrogen−hydrogen bonding has been shown to be a ubiquitous stabilizing interaction in angular polycyclic aromatic hydrocarbons and in several other organic molecules.[28] As another example, the 1,3-diaxial interaction in monosubstituted cyclohexanes has also been shown to arise from a subtle energetic balance. The energetic destabilization attributed to this steric interaction resides in the carbon skeleton which overrides the energetic stabilization due to the close H···H contacts.[29] It is concluded that a study of atomic energies complements the characterization of the bonding, since it allows one to uncover the local-atomic energies and their changes.

Finally, and as already mentioned, the electron density determined at the BCP, $\rho_{BCP}(\mathbf{r})$, is a measure of the strength of bonding between the two atoms and, thus, is related to the bond order (BO). An exponential expression has been proposed to describe this relationship:[14]

$$\mathrm{BO} = \exp[a(\rho_{\mathrm{BCP}} - b)] \tag{5}$$

where a and b are constants characterizing each specific type of bonding. The bond order signifies the number of electron pairs *shared* between the two bonded atoms. The sharing of electrons between two atoms is measured by the delocalization index which is the magnitude of the exchange of the electrons in the basin of atom A with those in the basin of atom B:[30]

$$\delta(\mathrm{A,B}) = 2|F^{\alpha}(\mathrm{A,B})| + 2|F^{\beta}(\mathrm{A,B})| \tag{6}$$

where

$$F^{\sigma}(\mathrm{A,B}) = -\sum_i \sum_j \int_{\mathrm{A}} d\mathbf{r}_1 \int_{\mathrm{B}} d\mathbf{r}_2 \{\phi_i^*(\mathbf{r}_1)\,\phi_j(\mathbf{r}_1)\,\phi_j^*(\mathbf{r}_2)\,\phi_i(\mathbf{r}_2)\} = -\sum_i \sum_j S_{ij}(\mathrm{A})\,S_{ji}(\mathrm{B}) \tag{7}$$

where $S_{ij}(\mathrm{A}) = S_{ji}(\mathrm{A})$ denotes the overlap of a pair of spin orbitals over the region A and σ refers to α or β spin. The delocalization index is defined between any two atoms in a molecule, but when reported for atoms sharing a bond path and an IAS, that is, bonded atoms, it has been shown to be a measure of the bond order.[30,31] The bond order is, thus, reflected in both the total electron density at the BCP and the delocalization index between the two bonded atoms. These two measures have been found to be highly correlated in the case of strong C−C bonding in polycyclic aromatic hydrocarbons.[32] Thus, one can calibrate eq 5 using the delocalization index rather than arbitrarily assigned bond orders:[32]

$$\delta(\mathrm{A,B}) = \exp[a(\rho_{\mathrm{BCP}} - b)] \tag{8}$$

Atomic Energies

To complete the characterization of the bonding, we report the atomic energies of the fluorine atoms involved in the F···F bonding and show that these fluorine atoms are stabilized as a result of this bonding. We thus recap briefly the definition of atomic energies in this section. For mathematical derivations and a more complete discussion, the reader is referred to the original work by Bader reviewed in his book.[14]

In addition to the definition expressed in eq 3, the kinetic energy density can also be written as

$$K(\mathbf{r}) = -\frac{\hbar^2}{4m} N \int d\tau' \,[\Psi \nabla^2 \Psi^* + \Psi^* \nabla^2 \Psi] \tag{9}$$

which is known as the Schrödinger kinetic energy. The two forms of local kinetic energy density are related by

$$K(\mathbf{r}) = G(\mathbf{r}) - \frac{\hbar^2}{4m}\nabla^2\rho(\mathbf{r}) \tag{10}$$

Clearly, eq 10 implies that the kinetic energy is not well defined when integrated over an arbitrary volume, ω, since it does not have a unique numerical value ($K(\omega) \neq G(\omega)$ in general) due to the appearance of a generally nonvanishing term proportional to the Laplacian of the density in the right-hand side of eq 11:

$$K(\omega) = G(\omega) - \frac{\hbar^2}{4m} N \int_{\omega} d\tau' \,\nabla\cdot\nabla\rho \tag{11}$$

Using the divergence theorem, the volume integral in eq 11 can be transformed to a surface integral:

$$K(\omega) = G(\omega) - \frac{\hbar^2}{4m} N \oint dS(\omega, \mathbf{r})\,\nabla\rho\cdot\mathbf{n}(\mathbf{r}) \tag{12}$$

From eq 12, it is evident that the kinetic energy would only be well defined when the second term on the right-hand side vanishes, that is, for systems bounded by zero-flux surfaces (satisfying the boundary condition expressed in eq 1). Systems bounded by a zero-flux surface include the total system and special subsystems termed "proper open systems" such as atoms in molecules. Regions of space belonging to a proper open system will be referred to as Ω, to contrast it with an arbitrary region of molecular space, ω, which may or may not be bounded by a zero-flux surface. For a proper open system, and since the kinetic energy is now well defined, one can write

$$K(\Omega) = G(\Omega) = T(\Omega) \tag{13}$$

Since for a region of space bounded by a zero-flux surface the kinetic energy is "well defined" and since the integral of the Laplacian vanishes over such a region, the integral of the local statement of the virial theorem (eq 2) over the volume of an atom, Ω, in a molecule yields the atomic virial theorem:

$$-2T(\Omega) = \mathcal{V}(\Omega) \tag{14}$$

where $\mathcal{V}(\Omega)$ is the total atomic virial (basin virial + surface virial). The atomic virial theorem allows one to define the atomic electronic energy, $E_e(\Omega)$:

$$E_e(\Omega) = T(\Omega) + \mathcal{V}(\Omega) \tag{15}$$

For systems in electrostatic equilibrium, when there are no forces acting on the nuclei (Hellmann−Feynman forces), the virial equals the average potential energy of the molecule, that is, $\mathcal{V} = V$. Under this condition, eq 14 becomes

$$-2T(\Omega) = V(\Omega) \tag{16}$$

where $V(\Omega)$ is the potential energy of atom Ω, and eq 15 becomes

$$E(\Omega) = E_e(\Omega) = T(\Omega) + V(\Omega) = -T(\Omega) \tag{17}$$

where $E(\Omega)$ is the total energy of atom Ω. Thus, it is because of the atomic statement of the virial theorem that, for an equilibrium geometry, where the forces on the nuclei vanish, the electronic energy of an atom is equal to the total energy of this atom, that is, $E_e(\Omega) = E(\Omega)$. This result is truly remarkable; it represents a quantum mechanical spatial partitioning of all of the interactions in a molecule—electronic−nuclear, electronic−

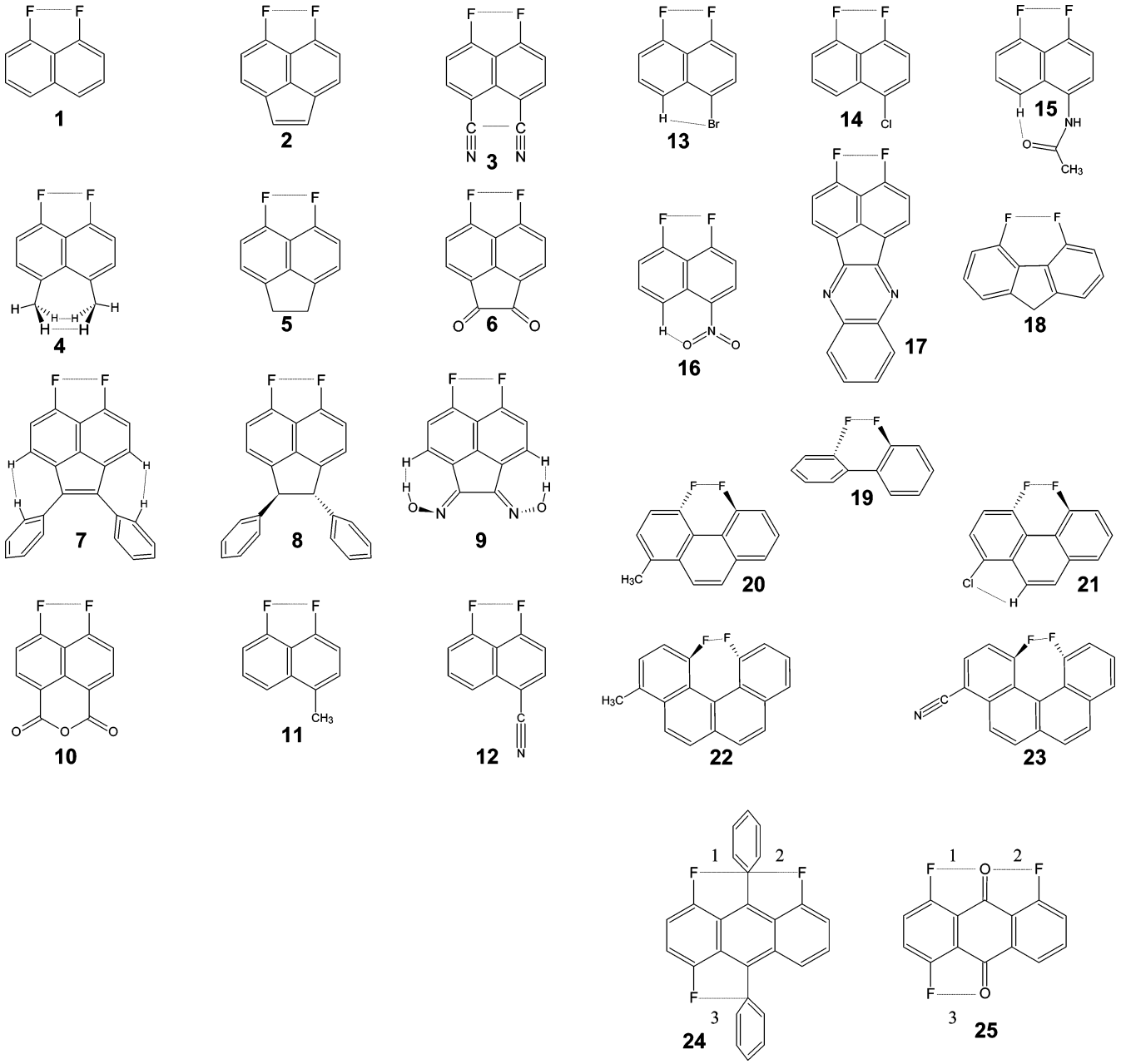

Figure 1. Chemical structures of the compounds constituting the data set employed in this study. Closed-shell bonding interactions are denoted by faint lines.

electronic, and nuclear−nuclear—into a sum of atomic contributions, a sum yielding the total energy of the molecule.

Computational Details

The geometries of all molecules have been optimized without constraints at the B3LYP/6-31G(d) level and frequencies calculated at that level to ensure that local minima have been located. Single-determinant Kohn−Sham "wave functions"[33] were obtained at the B3LYP/6-311++G(d,p)//B3LYP/6-31G(d) level. All electronic structure calculations were performed using the Gaussian 03 package.[34] The resulting electron densities were analyzed using the AIMPAC suite of programs[35,36] to obtain the bond and atomic properties and to prepare the contour and gradient vector field plots. The molecular graphs were plotted using AIM2000.[37,38] The AIMDELOC[39] program was used to calculate the delocalization indices from the atomic overlap matrices. Statistical analyses and correlations were carried out using the Origin 6.1[40] and the Polymath 5.1[41] packages.

Results and Discussion

Part I: F···F Interactions. *Optimized Geometries and F−F Internuclear Separations.* Figure 1 displays the set of molecules included in this study. All F···F and other closed-shell interactions are depicted by faint lines. Compounds **1**−**17** are all derivatives of 1,8-difluoronaphthalene (1,8-DFN), the numbering scheme of which is depicted in Figure 2. Contrary to what one might expect, the substituents have a significant effect on the F−F distance. The F−F distance falls within the range from 2.492 Å (in compound **4**) to 2.772 Å (in compound **2**), spanning almost 0.3 Å. This distance depends on the nature of the substituents at the 4 and 5 positions of naphthalene. Thus, in compound **4**, the naphthalene ring distorts to accommodate the bulky 1,4-dimethyl substituents, while, in **2**, the two fluorines

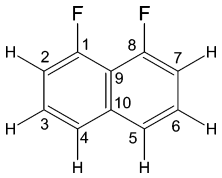

Figure 2. Numbering scheme for the naphthalene ring system exemplified on the 1,8-difluoronaphthalene molecule.

are pulled apart due to the participation of C4 and C5 in a strained five-membered ring.

In compounds **1**−**17**, a strong correlation was found between the improper C1−C10−C8 angle, which can be thought of as a "pair of scissors" and the F···F distance. In the parent compound 1,8-DFN (compound **1**), this angle is 62°, but in **4**, it is only 60° with a consequent shortening of the F−F distance. At the other extreme, the C1−C10−C8 angle opens to 66° in compound **2**, since the C4−C10−C5 moiety is part of a five-membered ring, driving the two fluorine atoms apart to their maximal separation. The other molecules fall between these two extremes. In all cases, the scissors angle turns out to be an excellent predictor of the F−F separation in compounds **1**−**17**, as can be seen in Figure 2.

Compounds **1**−**17** are characterized by planar naphthalene ring systems and two C−F bonds that are coplanar with the naphthalene rings and essentially parallel to each other. In contrast, compounds **18**−**23** are no longer derivatives of naphthalene and the two C−F bonds are no longer parallel. Compounds **19**−**23** further differ in that their two C−F bonds are also no longer coplanar, since these are highly crowded molecules which twist to accommodate the two proximal fluorine atoms. No F···F bond paths are present in **24** and **25** which thus do not exhibit F···F bonding interactions. Instead, F···C and F···O bond paths were found in these two compounds and will be discussed separately in part II of this section.

F···F Bond Path. As mentioned in the Introduction, the bond path is a unique and universal indicator of bonding interactions.[15] Bonding is an all or nothing phenomenon, but wherever a bond path links two nuclei, it is always locally stabilizing in an equilibrium geometry.[27] In general, the set of bond paths defining a molecular structure, the molecular graph, reproduces the conventional Lewis structure. In addition, one of the major advantages of the bond path as an indicator of bonding is that it is capable of the detection of weak interactions of any type: van der Waals, hydrogen bonding, dihydrogen bonding, and so forth. The literature is rich with descriptions of topologically characterized nonconventional bonding. Examples of bonding interactions which were reported on the basis of the topology of the electron density include the following: (1) the bonding between two equivalent or similar closed-shell hydrogen atoms (C−H···H−C), better termed hydrogen−hydrogen bonding interaction[28] to distinguish it from the dihydrogen bonding in which one hydrogen atom plays the role of the acceptor in the hydrogen bonding; [10,42,43] (2) bonding involving two nonequivalent hydrogen atoms or dihydrogen bonding ($X-H^{\delta+}\cdots H^{\delta-}-Y$);[44−46] (3) a plethora of hydrogen bonding interactions (see, for example, refs 12 and 47−53); (4) Cl···Cl closed-shell interactions in crystalline chlorine;[8] (5) a N═O···O═N closed-shell interaction;[54] (6) weak F···O and F···F′ intra- and intermolecular interactions;[9,12] (7) intramolecular F···F interactions;[10,11] (8) metallic closed-shell interaction between two Mn atoms;[55] and (9) several closed-shell O···O and O···C interactions.[55] The absence of a bond path has also been shown to be a decisive indicator for the lack of bonding despite an unusually close spatial arrangement of a closed-shell carbon atom to a titanium atom.[21]

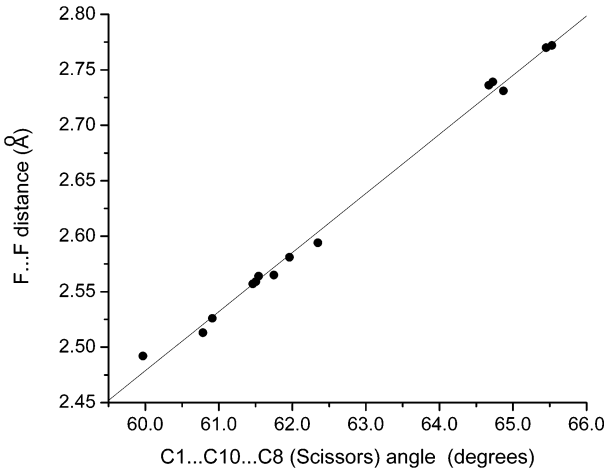

Figure 3. Regression plot showing the correlation between the scissors angle (the C1−C10−C8 angle) and the F···F distance (see text).

In this paper, we describe one of these examples of a closed-shell interaction in detail, an interaction which we show to be ubiquitous in crowded fluorinated compounds: the F···F bonding interaction.

Figure 4a is a contour map of the electron density of 1,8-difluoronaphthalene (1,8-DFN) in the molecular plane, Figure 4b is the corresponding gradient vector field showing the lines of steepest ascent in the electron density, and Figure 4c is a plot of the Laplacian showing regions of charge concentration and charge depletion. Superimposed on these plots are the sets of bond paths linking the nuclei as well as the intersections of the interatomic zero-flux surfaces with the molecular plane (some of these surfaces are indicated with arrows in the figure). Some atomic basins are colored in Figure 4 to highlight their respective forms. Basin F1, which shares a bond path and an IAS of zero flux with F8, is highlighted in yellow in the figure. F1 shares an IAS with F8 and with C1, and F8 shares an IAS with F1 and C8. We will denote the IAS from now on by the vertical bar "|" between the two bonded atoms sharing that surface. For example, the IAS between F1 and C1 will be denoted by "F1|C1" when we refer to the side of the surface facing the F1 basin and "C1|F1" when we refer to the side facing the C1 basin. The C1 atomic basin is surrounded by three IASs corresponding to its three bonding interactions: C1|F1, C1|C2, and C1|C9. The atomic basin of C1 extends to infinity tailing between the F1 and C2 basins but ends abruptly at the line where the basins of F1, C1, C9, C8, and F8 all meet, namely the ring critical point. In contrast, Figure 4 shows that the basin of C4, also highlighted in yellow, surrounds the H4 basin (in the plane of the figure) and extends to infinity on both of its sides. The same is true by symmetry for C5 and H5. Thus, unlike F1 and F8 which share an IAS, H4 and H5 are separated by the tailing atomic basins of C4, C5, and C10. From this discussion, it is also clear that the basins of C9 and C10 differ in a fundamental way: C9 is the only internal atom with finite boundaries totally enclosed within this molecule in the molecular plane, while C10 and all other atomic basins are external atoms extending to infinity.

A comparison of the Laplacian plot Figure 4c shows that the F···F interaction exhibits the same characteristics of typical closed-shell interactions (see Figure 7.15 on p 294 of Bader's book[14]). The Laplacian plots of closed-shell and shared interactions differ radically. Thus, for a shared interaction, the valence shell charge concentrations (VSCCs) of two atoms fuse into a

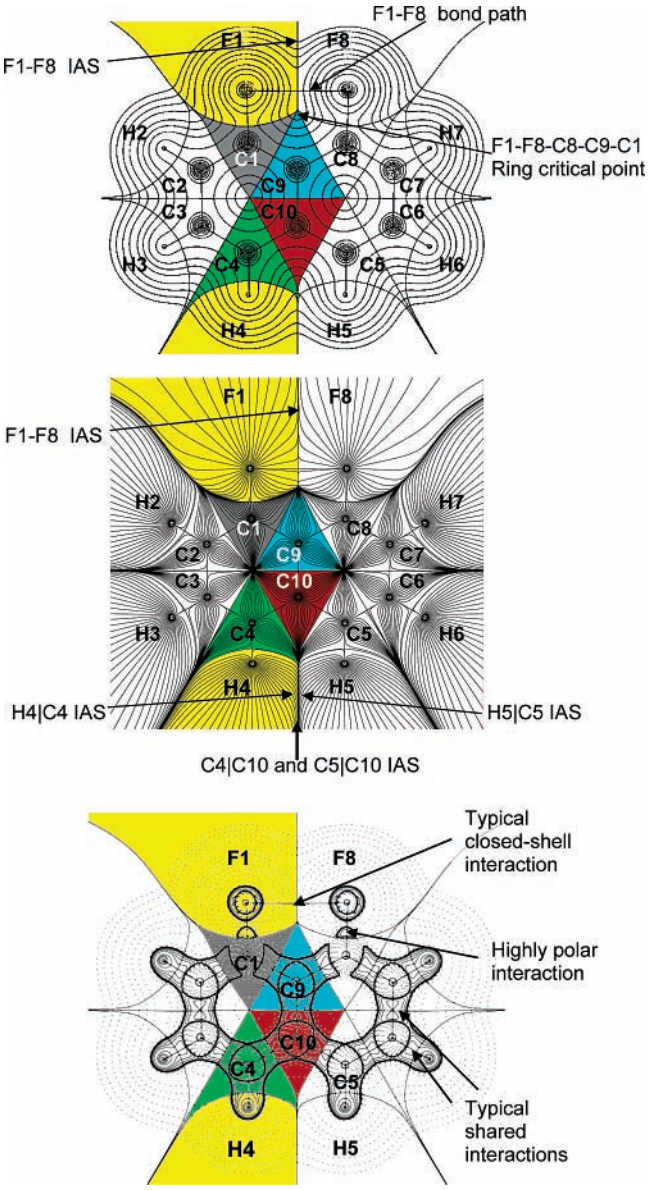

Figure 4. (a) Electron density contour plot of 1,8-difluoronaphthalene in the molecular plane. The set of contours from outside going inward have the following values: 0.001, 0.002, 0.004, 0.008, 0.02, 0.04, 0.08, 0.2, 0.4, 0.8, 2.0, 4.0, 8.0, 20.0, 40.0, and 80.0 au, respectively. (b) Gradient vector field corresponding to the contour plot. (c) Laplacian plot in the molecular plane. The solid contours denote regions of charge concentration where $\nabla^2\rho(\mathbf{r}) < 0$, and the dashed contours denote regions of charge depletion where $\nabla^2\rho(\mathbf{r}) > 0$. Contour levels increase or decrease from a zero contour in steps: ± 0.001, ± 0.002, ± 0.004, ± 0.008, ± 0.02, ± 0.04, ± 0.08, ± 0.2, ± 0.4, ± 0.8, ± 2.0, ± 4.0, ± 8.0, ± 20.0, ± 40.0, and ± 80.0 au, respectively. Several atoms have been colored for the easy distinction of the form of their atomic basins (see text).

continuous region of charge concentration between the atoms. In a closed-shell interaction, on the other hand, the valence shells for the atoms are clearly defined inside the basin of the two bonded atoms. The reader is asked to compare the bonding region between the two fluorine atoms in Figure 4c with that between any two carbon atoms or any carbon atom and its bonded hydrogen atom.

The F···F bond paths have been traced in all compounds **1**−**23** as can be seen from their molecular graphs plotted in Figure 5a,b. Figure 5c depicts the molecular graphs of compounds **24** and **25** which show closed-shell weak interactions of the type F···C (in **24**) and F···O (in **25**), interactions which will be discussed in part II below. In all cases, the corresponding ring critical point(s) has (have) also been located and the Poincaré−Hopf (P−H) relationship verified. This relationship, when stated for an isolated molecule, is[14]

$$\text{number of NCP} - \text{number of BCP} + \text{number of RCP} - \text{number of CCP} = 1 \quad (18)$$

where NCP stands for nuclear critical point, BCP for bond critical point, RCP for ring critical point, and CCP for cage critical point. Compounds **22** and **23** have been found to possess an unusual topology with highly twisted α-helical rings formed as a result of the F···F bonding interaction that gives rise to two ring critical points and a cage critical point. The P−H relationship has also been verified for these highly unusual ring topologies. The interesting topology of these rings is known to be a mathematical possibility[14] but has not been found previously in an actual molecular system to the best of our knowledge. This topic will be the subject of a separate study.[56]

Characterization of the F···F Bonding Interaction. Table 1 lists the bond properties of the F···F interactions in compounds **1**−**23**. In all cases, it is clear that this is a closed-shell interaction:

(1) The F···F internuclear distance is in the range ∼2.39−2.77 Å, in other words, generally smaller than (or close to) twice the van der Waals radius of fluorine (2.7 Å),[7] and thus can be classified as "close contact".[5] In all cases, the curvature of the bond path is rather small, as can be seen visually in Figure 5a,b or from the difference between the geometric bond length and the bond path length (BPL), Table 1, with a maximal difference of ∼0.08% of the bond length.

(2) ρ_{BCP} ranges from ∼0.022 to ∼0.010 au, values an order of magnitude smaller than that for a typical covalent bond. The small value of ρ_{BCP} for the F···F bonding is similar to moderate hydrogen bonding for which ρ_{BCP} ranges from ∼0.034 au in H3N···HF to ∼0.007 au in HCl···HF.[49]

(3) $\nabla^2\rho_{BCP} > 0$, since the Laplacian is dominated by λ_3, the positive curvature tangent to the bond path, for such a closed-shell interaction (compare the magnitudes of λ_3 with those of λ_1 and λ_2 in Table 1). $\nabla^2\rho_{BCP}$ ranges from ∼ +0.11 to ∼ +0.04 au, indicating very little sharing between the two atomic basins, which leads one to anticipate small delocalization between the basins of the two fluorine atoms.

(4) The delocalization index $\delta(F, F')$ indicates indeed very little sharing between the atomic basins of the two fluorine atoms. In the absence of charge transfer between two bonded atoms, one can equate the delocalization index between them to a bond order.[30,31] There is little or no charge transfer between the two fluorine atoms in these compounds (even when the two fluorine atoms are not equivalent by symmetry), and therefore, the delocalization index can be interpreted as the F···F bond order. From Table 1, we can see that the largest bond order (in **20**) is only ∼0.09, only 0.09 pair of electrons is shared between the two fluorine atoms, but this value can be as low as 0.04 pair for compound **2**. The delocalization indices have been previously shown to depend on both the internuclear separation and the angular disposition of the two F−C bonds.[13]

(5) As stated in the Introduction, the total energy density (eq 4) evaluated at the BCP, H_{BCP}, is negative when significant sharing of electrons dominates the interaction. In these cases, the potential energy density dominates the kinetic energy density at the BCP. From Table 1, one can see that the F···F interaction is dominated by the kinetic energy density (which is positive everywhere) and H_{BCP} is therefore always positive for this

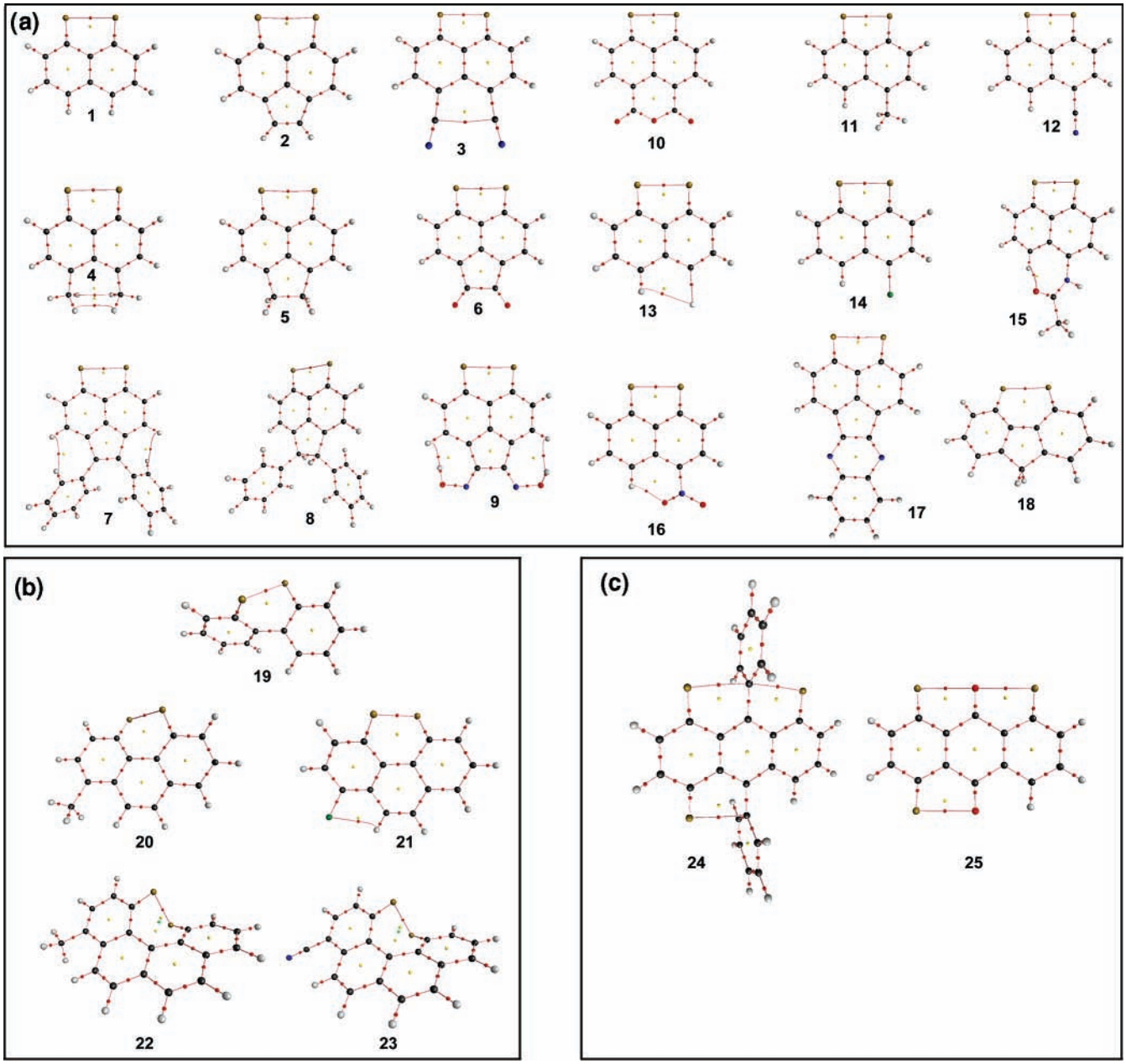

Figure 5. Computed molecular graphs of the set of compounds presented in Figure 1. (a) Compounds in which the F···F bond is essentially coplanar with the molecular plane; (b) crowded twisted molecules; (c) compounds devoid from F···F bonding but involving F···C and F···O closed-shell interactions. The red dots on bond paths are the bond critical points (BCPs), the yellow dots are the ring critical points (RCPs), and the green dots are cage critical points (CCPs). The spheres denote the positions of atoms: C = dark gray, O = red, N = dark blue, H = gray, F = golden yellow, Cl = green, Br = light gray (the reader is encouraged to also refer to Figure 1 to identify the different atoms and bonds). The planes of some of the molecules have been tilted to show the structure more clearly which results in the distortion of the proportions caused by perspective projection (e.g., some symmetry equivalent parts may appear to have different sizes). Also, the molecular graphs of different compounds are not necessarily plotted to the same scale.

interaction, as anticipated for a closed-shell interaction with little sharing of electrons.

(6) For weak interactions, the ellipticity indicates the stability of the bond critical point with respect to small geometrical changes such as those occurring during molecular vibration. From Table 1, the values of ϵ fall between ~0.66 and ~0.03, indicating relatively stable critical points which can also be concluded on the basis of the relatively large distance between the F···F BCPs and their respective ring critical point ensuing from the bonding (the separation between the RCP and the BCP is typically around 0.7 Å).

From the above considerations, we conclude that a weak F···F bonding interaction exists in these compounds, an interaction which exhibits the hallmarks of a typical weak closed-shell bonding interaction.

Correlations among the F···F Bond Properties. The properties characterizing the F···F bonding reported in Table 1 are highly correlated among themselves within the range of bond lengths studied (2.4−2.8 Å). Some of those correlations are displayed in Figures 6−9. Figure 6 shows the correlation between the internuclear distance (bond length) and several properties. From this figure, it is clear that ρ_{BCP} of this weak closed-shell F···F interaction decreases with distance, Figure 6a. Figure 6b shows that the delocalization index decreases with distance in a similar manner as ρ_{BCP}. Figure 6c shows a decrease in the Laplacian at the BCP as a function of the internuclear

TABLE 1: F···F Bond Properties[a]

cpd	δ(F, F′)	rFF′	BPL	ρ_{BCP}	$\nabla^2\rho_{BCP}$	G_{BCP}	$\mathcal{V}_{BCP}$	H_{BCP}	λ_1	λ_2	λ_3	ϵ
1	0.0578	2.5810	2.5816	0.0146	0.0645	0.0152	−0.0142	0.0010	−0.0150	−0.0137	0.0931	0.0930
2	0.0374	2.7721	2.7743	0.0096	0.0434	0.0100	−0.0091	0.0009	−0.0092	−0.0055	0.0582	0.6639
3	0.0659	2.5128	2.5133	0.0169	0.0766	0.0178	−0.0165	0.0013	−0.0178	−0.0170	0.1114	0.0474
4	0.0704	2.4916	2.4921	0.0178	0.0813	0.0189	−0.0175	0.0014	−0.0188	−0.0183	0.1183	0.0280
5	0.0410	2.7357	2.7370	0.0104	0.0463	0.0108	−0.0100	0.0008	−0.0101	−0.0072	0.0636	0.4121
6	0.0404	2.7314	2.7328	0.0104	0.0467	0.0108	−0.0100	0.0008	−0.0102	−0.0071	0.0640	0.4402
7	0.0375	2.7702	2.7721	0.0096	0.0435	0.0100	−0.0092	0.0009	−0.0092	−0.0056	0.0584	0.6570
8	0.0406	2.7394	2.7407	0.0103	0.0461	0.0107	−0.0099	0.0008	−0.0100	−0.0070	0.0631	0.4347
9	0.0424	2.7120	2.7132	0.0109	0.0484	0.0113	−0.0105	0.0008	−0.0107	−0.0079	0.0671	0.3624
10	0.0550	2.5943	2.5949	0.0141	0.0624	0.0146	−0.0137	0.0010	−0.0145	−0.0129	0.0897	0.1199
11	0.0602	2.5638	2.5643	0.0152	0.0672	0.0158	−0.0148	0.0010	−0.0156	−0.0145	0.0974	0.0763
12	0.0592	2.5655	2.5660	0.0151	0.0669	0.0157	−0.0147	0.0010	−0.0156	−0.0144	0.0969	0.0828
13	0.0607	2.5573	2.5578	0.0154	0.0684	0.0160	−0.0150	0.0010	−0.0159	−0.0148	0.0991	0.0737
14	0.0605	2.5589	2.5595	0.0153	0.0680	0.0160	−0.0150	0.0010	−0.0158	−0.0148	0.0986	0.0728
15	0.0606	2.5600	2.5605	0.0153	0.0679	0.0159	−0.0149	0.0010	−0.0158	−0.0147	0.0984	0.0759
16	0.0644	2.5262	2.5267	0.0164	0.0739	0.0173	−0.0161	0.0012	−0.0172	−0.0163	0.1075	0.0519
17	0.0391	2.7497	2.7513	0.0100	0.0451	0.0104	−0.0096	0.0008	−0.0097	−0.0064	0.0612	0.5193
18	0.0605	2.3884	2.6318	0.0130	0.0557	0.0131	−0.0124	0.0008	−0.0143	−0.0133	0.0833	0.0759
19	0.0460	2.3872	2.6736	0.0118	0.0522	0.0123	−0.0115	0.0008	−0.0111	−0.0106	0.0740	0.0469
20	0.0902	2.4916	2.3884	0.0222	0.1085	0.0247	−0.0222	0.0025	−0.0260	−0.0251	0.1597	0.0350
21	0.0902	2.4875	2.3872	0.0223	0.1088	0.0247	−0.0223	0.0025	−0.0261	−0.0252	0.1601	0.0341
22	0.0644	2.6730	2.4927	0.0177	0.0864	0.0197	−0.0178	0.0019	−0.0170	−0.0137	0.1170	0.2422
23	0.0650	2.6311	2.4886	0.0178	0.0870	0.0198	−0.0179	0.0019	−0.0172	−0.0140	0.1182	0.2330
max	0.0902	2.7721	2.7743	0.0223	0.1088	0.0247	−0.0091	0.0025	−0.0092	−0.0055	0.1601	0.6639
min	0.0374	2.3872	2.3872	0.0096	0.0434	0.0100	−0.0223	0.0008	−0.0261	−0.0252	0.0582	0.0280
av	0.0569	2.5991	2.6000	0.0144	0.0659	0.0153	−0.0141	0.0012	−0.0149	−0.0130	0.0938	0.2121
SD	0.0146	0.1146	0.1151	0.0036	0.0188	0.0042	0.0038	0.0005	0.0046	0.0053	0.0285	0.2056

[a] All entries are in atomic units except bond lengths and bond path lengths (BPLs) which are in angstroms, δ(F, F′) is the number of electron pairs shared between the two bonded fluorine atoms, and ϵ is dimensionless.

distance. The effects of the intenuclear distance on the energy densities at the BCP are displayed in Figure 6d−f. The kinetic energy density at the BCP decreases with the intenuclear distance (Figure 6d), but the potential energy density shows an opposing trend, as it becomes less stabilizing with an increase in the distance (Figure 6e). The behavior of the total energy is dominated by the behavior of the kinetic energy which decreases with increasing internuclear distance (Figure 6f).

Figure 7 shows the correlation of the electron density at the BCP with the delocalization index (Figure 7a) and with the energy densities (Figure 7b−d). The delocalization index increases linearly with ρ_{BCP}, indicating more delocalization and more accumulation of electron density at the BCP. The kinetic energy density increases with increasing ρ_{BCP} (Figure 7b), while the potential energy density becomes more negative with ρ_{BCP} (Figure 7c). There is a net increase in the total energy density at the BCP as ρ_{BCP} increases.

Figure 8a−c displays the correlations between the delocalization index and the energy densities. Since ρ_{BCP} and δ(F, F′) are highly positively correlated linearly (Figure 7a), the energetic trends as functions of δ(F, F′) are similar to those as functions of ρ_{BCP} plotted in Figure 7b−d. From Figure 7b−d and Figure 8, one concludes that the more there is accumulation of electron density at the BCP the more there is electron delocalization between the two fluorine atoms and the more the interaction is dominated by the kinetic energy density. Thus, while an increase in delocalization and in ρ_{BCP} is accompanied by an increasingly stable potential energy density (more negative), this stabilization is overwhelmed by the increase in the kinetic energy density for the F···F closed-shell interaction. These trends are the reverse of those described for a typical strong shared interaction such as the C−C bond where the total energy at the BCP drops with increasing electron delocalization as well as with increasing electron accumulation at the BCP (see Figure 1h of ref 32). This shows a fundamental difference in behavior between a weak closed-shell interaction such as the F···F bonding and a typical shared interaction.

Finally, Figure 8d shows the correlation between the difference between the bond path length and the bond length (the departure of the bond path from linearity) and the ellipticity. The plot shows a strong linear correlation between the two quantities, indicating that the larger the departure from linearity the larger the ellipticity.

Finally, we fitted our data to eq 8 to uncover whether the exponential relation which was shown to hold for strong covalent bonding[32] still holds in the case of the weak F···F closed-shell interaction. We obtained the following fitted equation:

$$\delta(\mathrm{F}, \mathrm{F}') = \exp[64.2532(\rho_{BCP} - 0.0595)] \qquad (19)$$

which yields $r^2 = 0.959$, showing that the relation holds even for this weak F···F interaction. The values of δ(F, F′) calculated from eq 19 are plotted against those calculated directly in Figure 9.

Energetic Consequences of F···F Bonding. As mentioned in the Introduction, it is a general finding of the theory of atoms in molecules that all bonding interactions are associated with a *local* stabilization even when the absence of such bonding in an isomer results in a lower *total* energy. To obtain an estimate of the stabilizing contribution of a F···F bonding interaction, we compare the atomic energies in each of the two isomers: 1,8-difluoronaphthalene (1,8-DFN), which contains one F···F bond path, and 1,5-difluoronaphthalene (1,5-DFN), which is devoid of such an interaction.

The total energy of 1,8-DFN, the one containing the F···F bonding interaction, is actually higher than the 1,5-DFN isomer by 3.5 kcal/mol. A comparison of the corresponding atomic energies (eq 17) in the two isomers explains this rather unexpected result. This comparison is given in the top panel of Figure 10. In the upper-left box of the figure (1,5-DFN), a

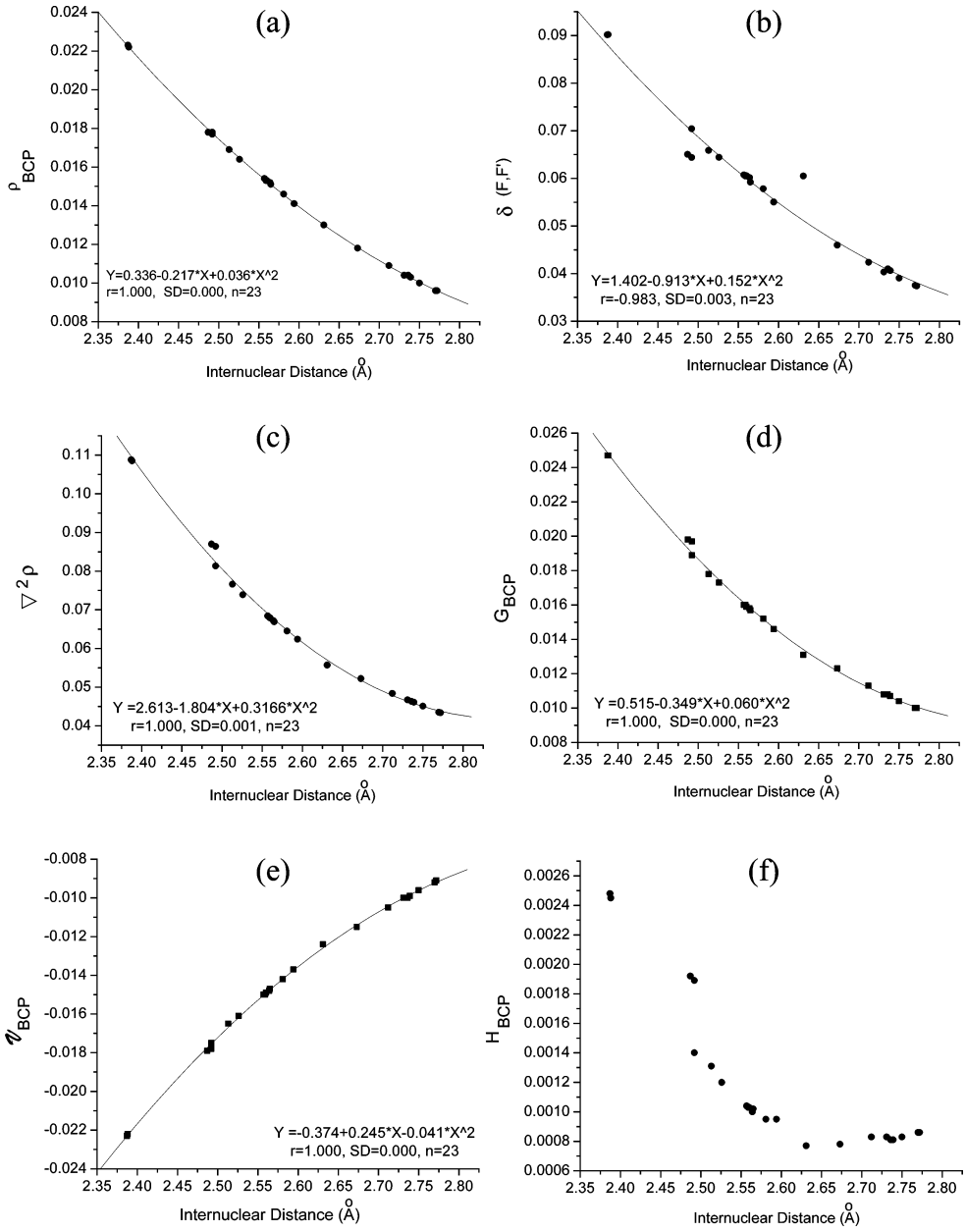

Figure 6. Series of plots representing the dependence of (a) ρ_{BCP}, (b) δ(F, F′), (c) $\nabla^2\rho_{BCP}$, (d) G_{BCP}, (e) V_{BCP}, and (f) H_{BCP} on the internuclear separation. All quantities in the plots are in atomic units except the internuclear distance which is in angstroms. No fit or statistical output is given for poor or irregular correlations.

relative atomic energy is defined as the difference between the energy of the atom in question and the energy of the most stable atom of the same element in the molecule. One can see that, in 1,5-DFN, C1 (and the equivalent C5) are the least stable carbon atoms in this molecule, with each being ∼178 kcal/mol less stable than atoms C9 or C10. The destabilization of C1 and C5 is due to a significant loss of electron population (∼0.46*e*) to the neighboring more electronegative fluorine atom, as can be seen from the comparison of atomic charges in the lower-left box of Figure 10 for this molecule. From the figure, one also finds that, in 1,5-DFN, C1 and C5 are the only atoms other than the two fluorine atoms with an appreciable net charge. The same is true about the charge distribution in 1,8-DFN, as can be seen from the lower-right box of Figure 10.

The upper-right box of Figure 10 displays the difference in the atomic energy between the two isomers defined as

$$\Delta E(\Omega) = E_{1,8-\mathrm{DFN}}(\Omega) - E_{1,5-\mathrm{DFN}}(\Omega) \qquad (20)$$

where Ω is a pair of equivalent atoms in the two isomers. The comparison shows that the fluorine atoms involved in the F···F interaction in 1,8-DFN are more stable (as expected) than the corresponding ones in 1,5-DFN by 7.2 kcal/mol each. In other words, the F···F interaction contributes ∼14 kcal/mol of stabilization to 1,8-DFN over 1,5-DFN. The overall destabilization of 1,8-DFN with respect to its isomer can be traced to the carbon skeleton, particularly C1 (and its symmetry equivalent C8) which is destabilized by 16.3 kcal/mol, C10 which is destabilized by 9.6 kcal/mol, and C9 which is destabilized by 3.2 kcal/mol. A bookkeeping of the differences in the atomic energies of the remaining atoms in the molecule (which are more stable in 1,8-DFN) yields the total energy differences between the two isomers, that is, $\sum_{\text{all atoms}} \Delta E(\Omega) = +3.4$ kcal/mol. The energetic destabilization of carbons 1, 8, 9, and 10 in 1,8-DFN with respect to 1,5-DFN can be the result of higher charge separation and more significant geo-

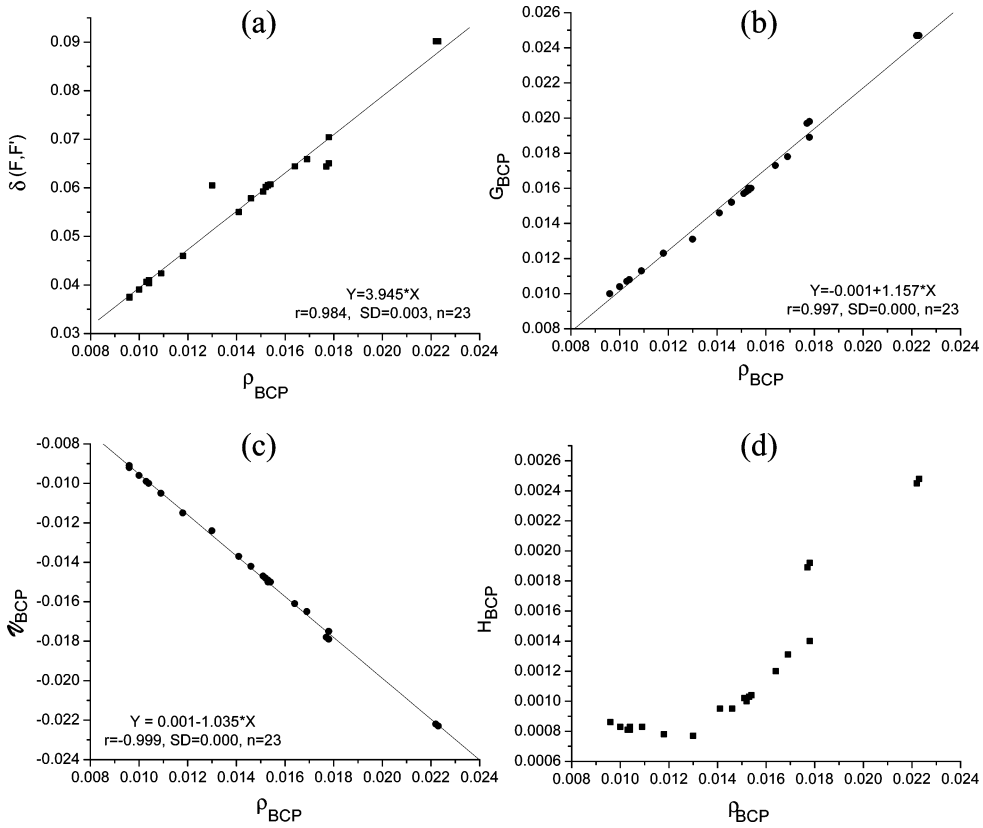

Figure 7. Series of plots representing the dependence of (a) δ(F, F′), (b) G_{BCP}, (c) $\mathcal{V}_{BCP}$, and (c) H_{BCP} on ρ_{BCP}. All quantities in the plots are in atomic units. No fit or statistical output is given for poor or irregular correlations.

metrical distortion of the ring system in 1,8-DFN to accommodate the two fluorine atoms in a relatively small space.

One cannot refer to the destabilization of C1, C8, C9, and C10 in 1,8-DFN relative to the corresponding atoms in 1,5-DFN as the result of a steric repulsion, since there are no forces operating in an equilibrium geometry. We must also caution from the erroneous identification of the *local* stabilization energy of ∼14 kcal/mol associated with the formation of a F···F bond path as a "bond energy": it is not. It is what it is: a local stabilization energy. In fact, one cannot define a bond energy for the F···F bond in these compounds, since this bond cannot be broken without the concurrent breaking of other bonds in the molecule.

To obtain an estimate for the F···F bond energy, we performed an MP2(full)/6-31+G(d) geometry optimization for a fluoromethane dimer, in head-to-head C_{3v} geometry ($H_3C-F\cdots F-CH_3$). The calculation reveals that there is no net binding, since a geometry optimization started with a F−F separation of 1.5 Å results in an ever increasing monomer−monomer separation. In a previous study, the interaction energy in the F−F···F−H dimer has been found to be ∼ −0.3 kcal/mol at three very different levels of theory (B3LYP/6-31G(d), B3LYP/6-311++G(d,p), and MP2/6-311++G(d,p)) and after correcting for basis set superposition error (BSSE).[12] The bond properties reported for the F−F···F−H complex at the MP2 level (rFF′ = 2.713 Å, ρ_{BCP} = 0.0073 au, $\nabla^2\rho_{BCP}$ = 0.0389 au)[12] compare well with one of the weakest F···F interactions reported in the present study, the interaction in compound **2** (see Table 1).

Part II: Other Nonconventional Closed-Shell Bonding Interactions. An examination of Figure 5 shows, besides the F···F bonding interactions, several other nonconventional bonding interactions revealed by the presence of bond paths. The bond properties of these interactions are collected in Table 2. A glance at the table reveals that these bonding interactions are weak to very weak, having ρ_{BCP} values ranging from ∼0.02 to ∼0.01 au. All of these interactions exhibit positive values for H_{BCP} as well as positive Laplacians at the BCP and can therefore be classified as closed-shell interactions. In all cases, these weak interactions result in ring(s) closure with the concurrent appearance of the ring critical point(s). The satisfaction of the P−H relationship (eq 18) has been verified for each molecular graph as mentioned previously. We shall now discuss each class separately.

F···C and F···O Interactions. Mallory et al.[57] describe two very interesting derivatives of anthracene (**24** and **25**) exhibiting unusually high fluorine−fluorine spin−spin coupling constants despite the presence of an intervening phenyl group in **24** and a carbonyl oxygen in **25** (see structures **24** and **25** in Figure 1 and the corresponding molecular graphs in Figure 5c). The three unusual bond paths traced in these two compounds have been labeled clockwise as bonds 1, 2, and 3 (see Figure 1). A comparison of all the bond properties of these six bonds reveals a striking similarity, even between the F···C and the F···O sets of bonds. Perhaps the most significant difference between the two sets is the difference between the internuclear distance and the bond path length. The difference averages to 0.003 Å for the F···C set and only 0.001 Å for the F···O set. The F···C set is therefore characterized by more curved bond paths, as we can also discern by the visual inspections of the molecular graphs of **24** and **25** in Figure 5c. Alkorta, Rozas, and Elguero report an interaction energy of −0.67 kcal/mol in the F−F···OH_2 complex at the MP2/6-311++G(d,p) level of theory after BSSE correction. The bond properties of this complex (rFF′ = 2.641 Å, ρ_{BCP} = 0.0221 au, $\nabla^2\rho_{BCP}$ = 0.0534 au)[12] are comparable with the F···O bond properties we reported in Table 1 for compound **25**. This similarity is particularly interesting because in the F−F···OH_2 complex the F···O

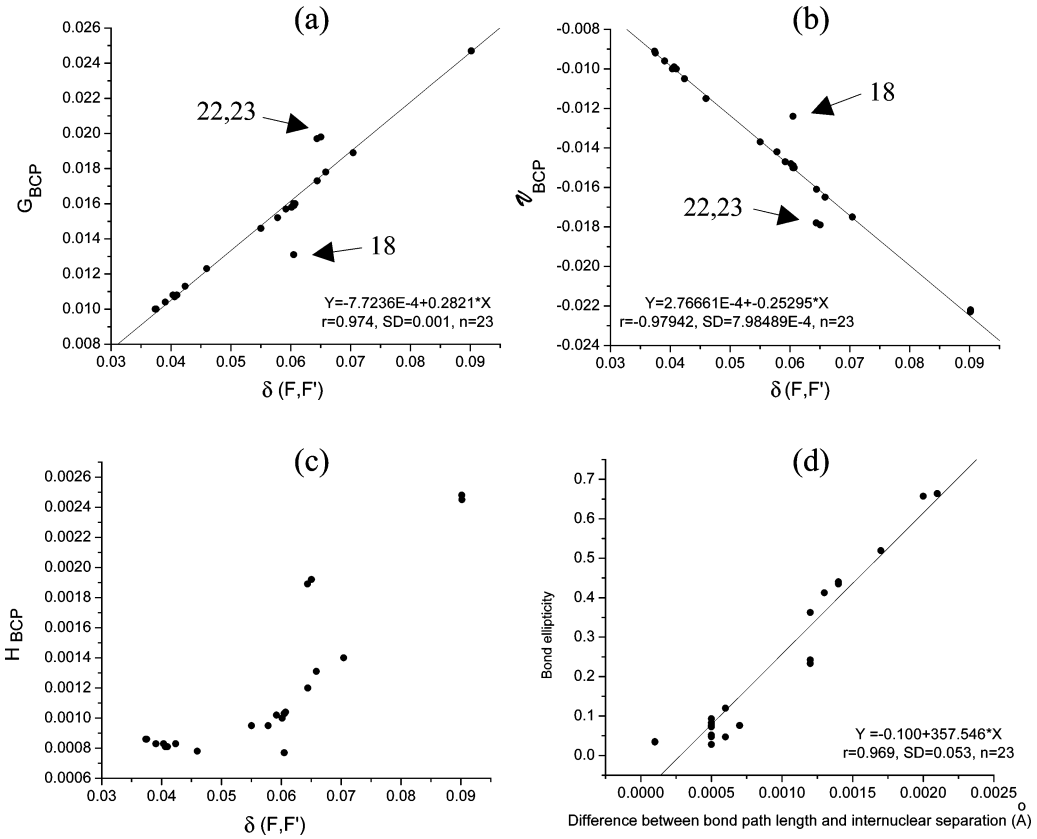

Figure 8. Series of plots representing the dependence of (a) G_{BCP}, (b) $\mathcal{V}_{BCP}$, and (c) H_{BCP} on the delocalization index between the two bonded fluorine atoms, δ(F, F′). All quantities in plots a−c are in atomic units. No fit or statistical output is given for poor or irregular correlations. The outliers have been indicated by the respective compound numbers in plots a and b. Plot d shows the correlation between a measure of the departure of the bond path from linearity (the difference between the internuclear separation and the bond path length, in angstroms) and the bond ellipticity.

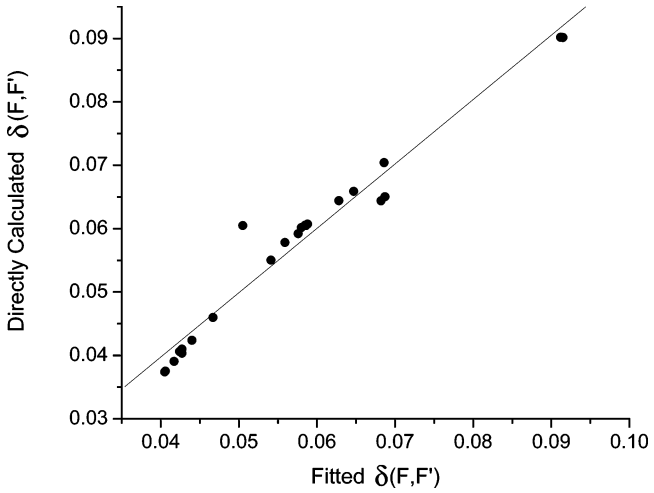

Figure 9. Plot of the values of δ(F, F′) calculated from ρ_{BCP} via eq 19 versus δ(F, F′) calculated directly.

distance is free to vary with no geometric constraints imposed by the rigidity of the molecular frame unlike in compound **25**. The same group also reports the results for the F−F···CO complex which at the BSSE-corrected MP2 level are rFF′ = 3.005 Å, ρ_{BCP} = 0.0062 au, and $\nabla^2\rho_{BCP}$=0.0268 au,[12] values indicating a significantly weaker interaction than we report here. Alkorta et al. report −0.33 kcal/mol for the F−F···CO interaction.

C···C Interaction. The two sp carbon atoms in compound **3** are separated by only ∼2.9 Å, much less than twice the van der Waals radius of carbon (3.5 Å).[5] The atoms are found to be bonded by a weak closed-shell interaction exhibiting a significantly curved bond path. The curvature of the bond path can be discerned from the molecular graph in Figure 5a as well as from the relatively large difference between the bond path length and the internuclear distance (∼0.01 Å).

C−H···X (X = Cl, Br), C−H···O═X (X = C, N), and C−H···H−X (X = C, O) Interactions. The last class of weak closed-shell bonding interactions found in this series of molecules includes hydrogen bonding (in compounds **13**, **15**, **16**, and **21**), dihydrogen bonding (in compound **9**), and hydrogen−hydrogen bonding (in compounds **4** and **7**). These provide further examples of such interactions already known and fully characterized in the literature.[28,42−46,48,49,52−53]

Conclusions

The F···F bonding interaction is likely to occur in polyfluorinated aromatic compounds when their internuclear separation is 2.3−2.8 Å despite the relative orientation of the two C−F internuclear axes and whether these are coplanar with the ring system or not. The presence of such bonding in 1,8-difluoronaphthalene (1,8-DFN) has been shown to impart ∼14 kcal/mol of stabilization *locally*, that is, to the two fluorine atoms involved in the bonding. The molecule is, however, *less* stable than its isomer 1,5-difluoronaphthalene (1,5-DFN) by ∼3 kcal/mol, an isomer that lacks this bonding interaction. The resolution of this apparent inconsistency is brought about by an atom-by-atom comparison of atomic energies between the two isomers. The estimate of the stabilization energy of the F···F bonding was obtained by comparing the atomic energies of the fluorine atoms in 1,8-DFN with the corresponding energies of the fluorine atoms in 1,5-DFN which lacks this interaction. Each of the fluorine atoms participating in the F···F interaction is

TABLE 2: Bond Properties of Nonconventional Weak Bonding Interactions[a]

cpd	A···B	*r*FF′	BPL	ρ_{BCP}	$\nabla^2\rho_{BCP}$	G_{BCP}	K_{BCP}	$\mathcal{V}_{BCP}$	H_{BCP}	λ_1	λ_2	λ_3	ϵ
24	F···C1	2.5997	2.6031	0.0175	0.0668	0.0155	−0.0011	−0.0144	0.0012	−0.0142	−0.0124	0.0933	0.1450
24	F···C2	2.6147	2.6184	0.0170	0.0648	0.0151	−0.0011	−0.0139	0.0012	−0.0137	−0.0119	0.0904	0.1522
24	F···C3	2.6126	2.6144	0.0169	0.0641	0.0149	−0.0011	−0.0138	0.0011	−0.0131	−0.0124	0.0896	0.0578
25	F···O1	2.5844	2.5850	0.0169	0.0722	0.0165	−0.0016	−0.0149	0.0016	−0.0166	−0.0154	0.1042	0.0833
25	F···O2	2.6211	2.6218	0.0157	0.0657	0.0151	−0.0013	−0.0138	0.0013	−0.0152	−0.0136	0.0945	0.1153
25	F···O3	2.6022	2.6029	0.0163	0.0689	0.0158	−0.0014	−0.0143	0.0015	−0.0159	−0.0144	0.0992	0.0992
3	C···C	2.8528	2.8767	0.0113	0.0385	0.0081	−0.0016	−0.0065	0.0016	−0.0085	−0.0052	0.0522	0.6455
13	H···Br	2.7108	2.8155	0.0133	0.0478	0.0100	−0.0019	−0.0081	0.0020	−0.0105	−0.0059	0.0643	0.7767
21	H···Cl	2.6095	2.7508	0.0136	0.0551	0.0113	−0.0025	−0.0089	0.0025	−0.0113	−0.0047	0.0710	1.4149
15	H···O	2.6615	2.8019	0.0085	0.0333	0.0070	−0.0014	−0.0056	0.0014	−0.0049	−0.0018	0.0399	1.6971
16	H···O	2.1344	2.1919	0.0208	0.0818	0.0176	−0.0029	−0.0147	0.0029	−0.0235	−0.0202	0.1255	0.1584
4	$H^{\delta+}\cdots H^{\delta-}$	2.1087	2.4115	0.0117	0.0430	0.0087	−0.0020	−0.0067	0.0020	−0.0107	−0.0049	0.0586	1.1876
7	$H^{\delta+}\cdots H^{\delta-}$	2.5062	3.4469	0.0065	0.0245	0.0048	−0.0013	−0.0035	0.0013	−0.0025	−0.0022	0.0293	0.1513
9	H···H	1.9128	2.1240	0.0145	0.0531	0.0112	−0.0020	−0.0092	0.0021	−0.0150	−0.0103	0.0784	0.4562

[a] All entries are in atomic units except bond lengths and bond path lengths (BPLs) which are in angstroms, and ϵ is dimensionless.

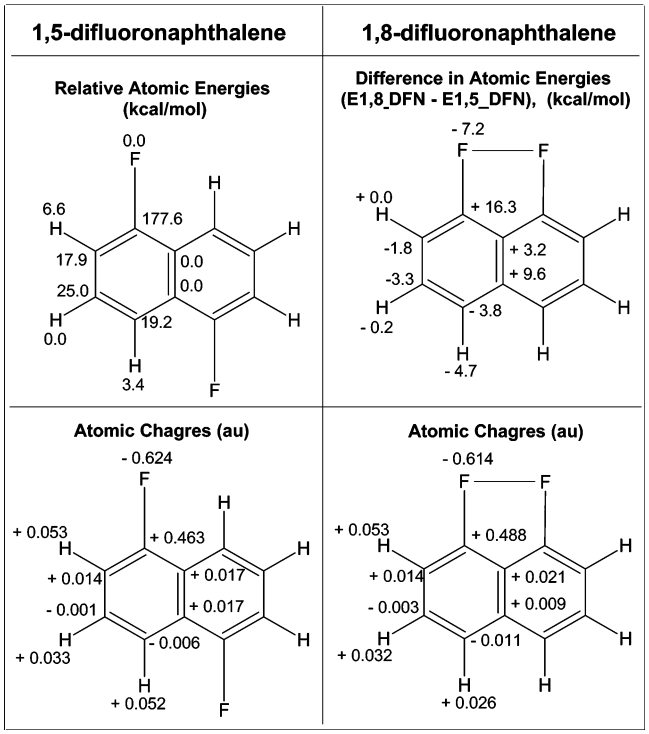

Figure 10. Comparison of the relative atomic energies (top panel) and atomic charges (lower panel) between the two isomers: 1,5-difluoronaphthalene (1,5-DFN) devoid of F···F interaction and 1,8-difluoronaphthalene (1,8-DFN) in which an F···F interaction occurs. The relative energies shown in the upper-left box for 1,5-DFN are given in kilocalories per mole and were calculated for each element taking the most stable atom of that element as the one with zero-relative atomic energy. The energies given for the 1,8-DFN isomer (upper-right box) are the difference between the atomic energy in that isomer and the corresponding atom in 1,5-DFN, given in kilocalories per mole. In 1,5-DFN, the absolute energy of a fluorine atom is −100.384 53 au, that of the most stable carbon C9 (or C10) is −38.089 82 au, and that of the most stable hydrogen H3 (or H7) is −0.610 07 au. The total energy of 1,5-DFN is −584.531 92 au, and that of 1,8-DFN is −584.526 37 au. The lower panel compares the AIM charges of the two isomers (in atomic units).

7.2 kcal/mol more stable than the corresponding fluorine atom in the isomer devoid of F···F bonding. On the other hand, the comparison also reveals that four carbon atoms in 1,8-DFN are significantly less stable than their counterparts in 1,5-DFN. The sum of these relative atomic stabilization and destabilization energies over all the atoms in the two isomers yields the net difference between the total molecular energies of the two isomers. The local stabilization associated with the F···F bond path should *not* be mistakenly identified as a bond energy, since the latter implies a bond dissociation. It is impossible to achieve the dissociation of an F···F bond in this series of molecules without the concurrent dissociation of other bonds.

Several other interesting nonclassical closed-shell interactions have also been found and characterized in these compounds including F···C, F···O, and C···C bonding as well as several variants of hydrogen bonding, dihydrogen bonding, and hydrogen−hydrogen bonding.

The present work is yet another testimonial as to the usefulness, power, and richness of the bond path concept[15] and of the theory of atoms in molecules[14] in general.

Acknowledgment. The authors acknowledge the Natural Sciences and Engineering Research Council of Canada (NSERC) for funding and the Killam Trusts for a Killam Postdoctoral Fellowship to one of them (C.F.M.).

Note Added in Proof. A report (ref. 58) of a discussion of O···F and F···F closed-shell bonding interactions in protonated perfluorodiethyl ether came to our attention after our paper was accepted for publication.

References and Notes

(1) Murray-Rust, P.; Stallings, W. C.; Monti, C. T.; Preston, R. K.; Glusker, J. P. *J. Am. Chem. Soc.* **1983**, *105*, 3206−3214.
(2) Sarma, J. A. R. P.; Desiraju, G. R. *Acc. Chem. Res.* **1986**, *19*, 222−228.
(3) Price, S. L.; Stone, A. J.; Rowland, R. S.; Thornley, A. E. *J. Am. Chem. Soc.* **1994**, *116*, 4910−4918.
(4) Ramasubbu, N.; Parthasarathy, R.; Murray-Rust, P. *J. Am. Chem. Soc.* **1986**, *108*, 4308−4314.
(5) Desiraju, G. R.; Parthasarathy, R. *J. Am. Chem. Soc.* **1989**, *111*, 8725−8726.
(6) Shimoni, L.; Carrell, H. L.; Glusker, J. P.; Coombs, M. M. *J. Am. Chem. Soc.* **1994**, *116*, 8162−8168.
(7) Pauling, L. *The Nature of the Chemical Bond*, 3rd ed.; Cornell University Press: Ithaca, NY, 1960.
(8) Tsirelson, V.; Zou, P. F.; Tang, T.-H.; Bader, R. F. W. *Acta Crystallogr., Sect. A* **1995**, *51*, 143−153.
(9) Bach, A.; Lentz, D.; Luger, P. *J. Phys. Chem. A* **2001**, *105*, 7405−7412.
(10) Grabowski, S. J.; Pfitzner, A.; Zabel, M.; Dubis, A. T.; Palusiak, M. *J. Phys. Chem. B* **2004**, *108*, 1831−1837.
(11) Alkorta, I.; Elguero, J. *Struct. Chem.* **2004**, *15*, 117−120.
(12) Alkorta, I.; Rozas, I.; Elguero, J. *J. Phys. Chem. A* **1998**, *102*, 9278−9285.
(13) Castillo, N.; Matta, C. F.; Boyd, R. J. *J. Chem. Inf. Mod.*, in press.
(14) Bader, R. F. W. *Atoms in Molecules: A Quantum Theory*; Oxford University Press: Oxford, U.K., 1990.
(15) Bader, R. F. W. *J. Phys. Chem. A* **1998**, *102*, 7314−7323.
(16) Runtz, G. R.; Bader, R. F. W.; Messer, R. R. *Can. J. Chem.* **1977**, *55*, 3040−3045.
(17) Bader, R. F. W.; Anderson, S. G.; Duke, A. J. *J. Am. Chem. Soc.* **1979**, *101*, 1389−1395.

(18) Bader, R. F. W.; Tal, Y.; Anderson, S. G.; Nguyen-Dang, T. T. *Isr. J. Chem.* **1980**, *19*, 8−29.
(19) Koritsanszky, T. S.; Coppens, P. *Chem. Rev.* **2001**, *101*, 1583−1628.
(20) Bader, R. F. W. *Phys. Rev. B* **1994**, *49*, 13348−13356.
(21) Bader, R. F. W.; Matta, C. F. *Inorg. Chem.* **2001**, *40*, 5603−5611.
(22) Bader, R. F. W.; Matta, C. F.; Cortés-Guzmán, F. *Organometallics* **2004**, *23*, 6253−6263.
(23) Boyd, R. J.; Edgecombe, K. E. *J. Am. Chem. Soc.* **1988**, *110*, 4182−4186.
(24) Boyd, R. J.; Boyd, S. L. *J. Am. Chem. Soc.* **1992**, *114*, 1652−1655.
(25) Bader, R. F. W.; Nguyen-Dang, T. T. *Adv. Quantum Chem.* **1981**, *14*, 63−123.
(26) Cremer, D.; Kraka, E. *Angew. Chem., Int. Ed. Engl.* **1984**, *23*, 627−628.
(27) Keith, T. A.; Bader, R. F. W.; Aray, Y. *Int. J. Quantum Chem.* **1996**, *57*, 183−198.
(28) Matta, C. F.; Hernández-Trujillo, J.; Tang, T. H.; Bader, R. F. W. *Chem.−Eur. J.* **2003**, *9*, 1940−1951.
(29) Cortés-Guzmán, F.; Hernández-Trujillo, J.; Cuevas, G. *J. Phys. Chem. A* **2003**, *107*, 9253−9256.
(30) Fradera, X.; Austen, M. A.; Bader, R. F. W. *J. Phys. Chem. A* **1999**, *103*, 304−314.
(31) Austen, M. A. *A New Procedure for Determining Bond Orders in Polar Molecules, with Applications to Phosphorus and Nitrogen Containing Systems.* Ph.D. Thesis, McMaster University, Hamilton, Canada, 2003.
(32) Matta, C. F.; Hernández-Trujillo, J. *J. Phys. Chem. A* **2003**, *107*, 7496−7504.
(33) Kohn, W.; Sham, L. J. *Phys. Rev. A* **1965**, *140* (4A), 1133−1138.
(34) Frisch, M. J.; Trucks, G. W.; Schlegel, H. B.; Scuseria, G. E.; Robb, M. A.; Cheeseman, J. R.; Montgomery, J. A., Jr.; Vreven, T.; Kudin, K. N.; Burant, J. C.; Millam, J. M.; Iyengar, S. S.; Tomasi, J.; Barone, V.; Mennucci, B.; Cossi, M.; Scalmani, G.; Rega, N.; Petersson, G. A.; Nakatsuji, H.; Hada, M.; Ehara, M.; Toyota, K.; Fukuda, R.; Hasegawa, J.; Ishida, M.; Nakajima, T.; Honda, Y.; Kitao, O.; Nakai, H.; Klene, M.; Li, X.; Knox, J. E.; Hratchian, H. P.; Cross, J. B.; Adamo, C.; Jaramillo, J.; Gomperts, R.; Stratmann, R. E.; Yazyev, O.; Austin, A. J.; Cammi, R.; Pomelli, C.; Ochterski, J. W.; Ayala, P. Y.; Morokuma, K.; Voth, G. A.; Salvador, P.; Dannenberg, J. J.; Zakrzewski, V. G.; Dapprich, S.; Daniels, A. D.; Strain, M. C.; Farkas, O.; Malick, D. K.; Rabuck, A. D.; Raghavachari, K.; Foresman, J. B.; Ortiz, J. V.; Cui, Q.; Baboul, A. G.; Clifford, S.; Cioslowski, J.; Stefanov, B. B.; Liu, G.; Liashenko, A.; Piskorz, P.; Komaromi, I.; Martin, R. L.; Fox, D. J.; Keith, T.; Al-Laham, M. A.; Peng, C. Y.; Nanayakkara, A.; Challacombe, M.; Gill, P. M. W.; Johnson, B.; Chen, W.; Wong, M. W.; Gonzalez, C.; Pople, J. A. *Gaussian 03*, revision B.01; Gaussian, Inc.: Pittsburgh, PA, 2003.
(35) Biegler-König, F. W.; Bader, R. F. W.; Tang, T.-H. *J. Comput. Chem.* **1982**, *13*, 317−328.
(36) Bader, R. F. W. *AIMPAC.* http://www.chemistry.mcmaster.ca/aimpac/.
(37) Biegler-König, F. W.; Schönbohm, J.; Bayles, D. *J. Comput. Chem.* **2001**, *22*, 545−559.
(38) Biegler-König, F. W.; Schönbohm, J.; Bayles, D. The AIM2000 program can be downloaded from the Internet at http://gauss.fh-bielefeld.de/aim2000.
(39) Matta C. F. *AIMDELOC*, program to calculate AIM localization and delocalization indices (QCPE0802); Quantum Chemistry Program Exchange, Indiana University, IN, 2001 (http://qcpe.chem.indiana.edu/).
(40) *Microcal. Origin v.6.0*; Microcal Software, Inc.: MA, 1999.
(41) Shacham, M.; Cutlip, M. B.; Elly, M. *POLYMATH 5.1*; CACHE Corporation: The University of Connecticut, Ben Gurion University of the Negev, and University of Michigan, 2000.
(42) Robertson, K. N.; Knop, O.; Cameron, T. S. *Can. J. Chem.* **2003**, *81*, 727−743.
(43) Wang, C.-C.; Tang, T.-H.; Wu, L.-C.; Wang, Y. *Acta Crystallogr., Sect. A* **2004**, *60*, 488−493.
(44) Popelier, P. L. A. *J. Phys. Chem. A* **1998**, *102*, 1873−1878.
(45) Grabowski, S. J. *J. Phys. Chem. A* **2000**, *104*, 5551−5557.
(46) Grabowski, S. J. *J. Phys. Chem. A* **2001**, *105*, 10739−10746.
(47) Calhorda, M. J. *Chem. Commun.* **2000**, 801−809.
(48) Alkorta, I.; Rozas, I.; Elguero, J. *Chem. Soc. Rev.* **1998**, *27*, 163−170.
(49) Carroll, M. T.; Bader, R. F. W. *Mol. Phys.* **1988**, *65*, 695−722.
(50) Cheeseman, J. R.; Carroll, M. T.; Bader, R. F. W. *Chem. Phys. Lett.* **1988**, *143*, 450−458.
(51) Koch, U.; Popelier, P. L. A. *J. Phys. Chem.* **1995**, *99*, 9747−9754.
(52) Knop, O.; Rankin, K. N.; Boyd, R. J. *J. Phys. Chem. A* **2001**, *105*, 6552−6566.
(53) Knop, O.; Rankin, K. N.; Boyd, R. J. *J. Phys. Chem. A* **2003**, *107*, 272−284.
(54) Zhurova, E. A.; Tsirelson, V. G.; Stash, A. I.; Pinkerton, A. A. *J. Am. Chem. Soc.* **2002**, *124*, 4574−4575.
(55) Bianchi, R.; Gervasio, G.; Marabello, D. *Inorg. Chem.* **2000**, *39*, 2360−2366.
(56) Castillo, N.; Matta, C. F.; Boyd, R. J. *Chem. Phys. Lett.* **2005**, submitted for publication.
(57) Mallory, F. B.; Mallory, C. W.; Baker, M. B. *J. Am. Chem. Soc.* **1990**, *112*, 2577−2581.
(58) Vila, A.; Mosquera, R. A. *J. Mol. Struct.* (THEOCHEM) **2001**, *546*, 63−72.